

Optimized Weighted Essentially Nonoscillatory Schemes for Linear Waves with Discontinuity

Z. J. Wang* and R. F. Chen†

*Department of Mechanical Engineering, Michigan State University, East Lansing, Michigan 48824;

and †Daimler Chrysler Corporation, Auburn Hills, Michigan 48083

E-mail: ZJW@egr.msu.edu

Received November 10, 2000; revised June 12, 2001

ENO (essentially nonoscillatory) and weighted ENO (WENO) schemes were designed for high resolution of discontinuities, such as shock waves, while optimized schemes such as the DRP (dispersion–relation–preserving) schemes were optimized for short waves (with respect to the grid spacing Δx , e.g., waves that are $6-8\Delta x$ in wavelength) in the wavenumber space. In this paper, we seek to unite the advantages of WENO and optimized schemes through the development of Optimized WENO (OWENO) schemes to tackle shock/broadband acoustic wave interactions and small-scale flow turbulences relative to the grid spacing. OWENO schemes are optimized in two levels. In the first level, optimized schemes are constructed for all candidate stencils by minimizing the error in the wavenumber space. In the second level, these optimized schemes are convexly combined using weights constructed to achieve not only higher order of accuracy but also high resolution for short waves. In addition, a new definition of smoothness indicators is presented for the OWENO schemes. These smoothness indicators are shown to have better resolution for short waves. A third-order OWENO scheme and a seventh-order WENO scheme are compared against each other for performance on the scalar model equation. It has been shown that the OWENO scheme indeed gives much better results in resolving short waves than the WENO scheme while yielding nonoscillatory solutions for discontinuities. Finally the OWENO scheme is extended to the linearized Euler equations to solve two computational aeroacoustics (CAA) benchmark problems to demonstrate its capability. © 2001 Elsevier Science

Key Words: optimized; WENO; CAA; CFD; shock; acoustic; high order.

1. INTRODUCTION

The past decade and a half has seen many impressive developments in computational aeroacoustics (CAA). As pointed out by Tam [22], aeroacoustic problems differ significantly from aerodynamic problems in their nature, characteristics, and objectives. They are

intrinsically unsteady, and the dominant frequencies are usually high. Therefore, the development of CAA algorithms needs independent thinking. As a result of this independent thinking, many powerful numerical algorithms have been developed to address the particular problems in CAA, e.g., the dispersion–relation–preserving (DRP) finite difference schemes [23] and other high-order algorithms [7, 10, 12, 16, 19]. The basic idea in DRP schemes is to optimize the scheme coefficients for the high resolution of short waves with respect to the computational grid, i.e., waves with wavelength of $6\text{--}8\Delta x$ (defined here as $6\text{--}8$ points-per-wave or PPW). Therefore, DRP schemes are also called optimized schemes.

The idea of optimizing the scheme coefficients to minimize a particular type of error instead of the truncation error has been used very successfully over the years by many researchers in designing a variety of optimized schemes [4, 11, 15, 26]. The rationale for optimizing numerical schemes for short waves is that in a broadband acoustic wave, there are both short and long wave components. For long waves, even lower-order schemes can do a decent job in resolving them. It is the short waves, however, which require high resolution if one is to resolve the broadband wave with as high accuracy as possible.

Other optimized schemes have also been developed successfully for CAA applications [27–29]. In the DRP schemes, central differences are employed to approximate the first derivative. They are, therefore, nondissipative in nature. Although nondissipative schemes are ideal for aeroacoustic problems, numerical dissipation is required to damp any non-physical waves generated by boundary and/or initial conditions. In practice, high-order dissipation terms are added to the DRP schemes to suppress spurious oscillations. The amount of artificial dissipation required is, however, problem dependent. One may need to fine-tune the artificial damping to obtain the best results for a particular problem at hand. To remedy this problem, optimized upwind DRP schemes have been developed more recently by Zhuang and Chen [27, 28], and Lockard, Brentner and Atkins [16]. Instead of using the central difference stencil, an upwind-biased stencil was selected based on the local wave propagating direction. Then the upwind schemes are optimized in the wavenumber space following the same idea of DRP schemes. The upwind DRP schemes are by design dissipative. Therefore, they are capable of suppressing spurious oscillations without the addition of extra artificial damping, relieving the user from fine-tuning the amount of numerical dissipation. Another advantage of the upwind DRP schemes is that acceptable results can be obtained even if the mean flow contains discontinuities. With both the DRP and upwind DRP schemes, it is very difficult to obtain oscillation-free numerical solutions if the mean flow is discontinuous, because the schemes are linear. For nonlinear shock-acoustic wave interaction problems, numerical oscillations may contaminate the resultant solutions and even diverge the simulations.

ENO (essentially non-oscillatory) schemes started with the classic paper of Harten *et al.* [6] and were designed for shock capturing. Before the birth of ENO schemes, several approaches were possible to suppress numerical oscillations. One approach was to add artificial dissipation [8]. The dissipation can be tuned to be large enough near discontinuities to suppress oscillations, but small elsewhere to maintain high-order accuracy. A disadvantage of the approach is that the dissipation terms are problem dependent. Another approach is to use limiters to eliminate oscillations [25]. The TVD schemes [5, 17] are such examples. One drawback of this approach is that the solution accuracy near extrema (even near smooth extrema) must degrade to first order, resulting in clipping of smooth extrema. The ENO schemes remedied the drawback of TVD schemes in that they are uniformly high-order accurate, yet essentially nonoscillatory for piecewise smooth solutions. More

recently, weighted ENO (WENO) schemes [9, 14, 21] were developed to further increase the order of accuracy, while resolving discontinuities with essentially no numerical oscillations. Many studies [1, 2] confirmed that ENO and WENO schemes are indeed uniformly high-order accurate, and capable of resolving shocks with high resolution. They have been successfully applied to problems with shocks and complex smooth flow structures, such as those occurring in shock interactions with turbulent flows, and shock/vortices interactions. Although ENO and WENO schemes are not designed for CAA, they have been applied to CAA problems because of their high order of accuracy. The direct applications of ENO and WENO to CAA problems are, however, not optimum because ENO and WENO schemes are designed for high resolution of discontinuities and to achieve a high formal order of accuracy, and NOT optimized for broadband acoustic waves. For short waves, ENO and WENO schemes suffer the same drawback as conventional maximum-order finite difference schemes in that they quickly lose resolution compared to optimized schemes.

In this paper, we seek to unite the advantages of both the optimized DRP schemes and WENO schemes in the development of Optimized WENO (OWENO) schemes. The idea is to optimize the WENO schemes in the wavenumber space, following the practice of the DRP schemes to achieve high resolution for short waves with about 6 PPW. At the same time, OWENO schemes will retain the advantages of WENO schemes in that discontinuities are captured with essentially no oscillations, and without any extra numerical damping. At least two groups of researchers [13, 26] attempted to optimize WENO schemes for short waves. In the approach presented in [13, 26], only the weights in the WENO schemes are optimized. Although it was also found in [26] that the smoothness indicators added significant numerical damping for short waves, no solutions were given there or in [13]. In this paper, optimizations are done in two levels. In the first level, optimized schemes for all candidate stencils are constructed. In the second level, optimizations are also performed to find the best weights to combine all the stencils. In addition, new smoothness indicators are presented for short waves. In the following section, we first review the concept behind optimized, ENO, and WENO schemes. Then OWENO schemes are derived for the linear wave equation, and their dissipative and dispersive behaviors are analyzed. After that, the extension of OWENO to the linear Euler equations is described, followed by a brief discussion on the time-marching method. Next, sample demonstration cases with 1-D scalar wave equation and the linearized Euler equations are carried out to evaluate the performance of OWENO schemes. Finally, conclusions from the study are summarized, and possible future work is outlined.

2. OVERVIEW OF OPTIMIZED, ENO, AND WENO SCHEMES

In the design of a traditional finite difference scheme, the usual practice is to maximize the order of accuracy of the numerical scheme given the size of the difference stencil. However, maximum-order schemes may not be the best for high-frequency short waves, as shown by Tam and Webb [23]. To present the basic idea, we will consider the scalar wave equation with a constant positive wave speed a ,

$$\frac{\partial u(x, t)}{\partial t} + a \frac{\partial u(x, t)}{\partial x} = 0 \quad \text{with } u(x, 0) = u_0(x), \quad (1)$$

where u is a state variable, $t > 0$ is time, and x is the Cartesian coordinate. We assume proper boundary conditions are available when necessary. Given a uniform grid $x_i = i \Delta x$,

$i = 0, \dots, N$ with a constant grid spacing Δx , we seek to develop a semi-discrete conservative numerical scheme approximating (1) in the form

$$\frac{\partial u_i}{\partial t} + \frac{a}{\Delta x} (\tilde{u}_{i+1/2}^r - \tilde{u}_{i-1/2}^r) = 0, \tag{2}$$

where u_i is a numerical approximation to $u(x, t)$ at grid point x_i and $\tilde{u}_{i+1/2}^r$ and $\tilde{u}_{i-1/2}^r$ are numerical fluxes (more precisely $a\tilde{u}_{i+1/2}^r$ is the flux) depending on k continuous grid points including x_i itself, i.e.,

$$\tilde{u}_{i+1/2}^r = \tilde{u}_{i+1/2}^r(u_{i-r}, \dots, u_{i+s}) = \sum_{j=0}^{k-1} c_{rj} u_{i-r+j}. \tag{3}$$

Here $r \geq 0, s \geq 0$, and $r + s + 1 = k$; k is the size of the stencil used to compute the numerical flux; and c_{rj} are constants independent of the solution. The coefficients c_{rj} can be determined through a Taylor expansion to achieve a maximum k th order accuracy, i.e., by satisfying

$$\frac{\partial u_i}{\partial x} = \frac{(\tilde{u}_{i+1/2}^r - \tilde{u}_{i-1/2}^r)}{\Delta x} + O(\Delta x^k). \tag{4}$$

The philosophy of optimized schemes is to sacrifice the formal order of accuracy for achieving better resolution for a wider range of wavenumbers, for short waves in particular. Instead of always achieving the maximum order of accuracy of k , we set to design a scheme with formal order of accuracy of p_1 with $p_1 < k$, i.e.,

$$\frac{\partial u_i}{\partial x} = \frac{(\tilde{u}_{i+1/2}^r - \tilde{u}_{i-1/2}^r)}{\Delta x} + O(\Delta x^{p_1}). \tag{5}$$

Using a Taylor expansion, we can derive p_1 equations about the coefficients c_{rj} . We need an extra $k - p_1$ equations to determine all the coefficients. The idea in the DRP schemes [23] is to minimize the difference between the numerical wavenumber and the actual wavenumber. Based on a Fourier analysis, the numerical wavenumber for (2) with the given stencil is found to be

$$\bar{\alpha}^r \equiv \frac{-\sqrt{-1}}{\Delta x} \sum_{j=-r}^s c_{r,j+r} \exp(\sqrt{-1}j\alpha\Delta x)[1 - \exp(-\sqrt{-1}\alpha\Delta x)] = \alpha + O(\alpha\Delta x)^{p_1}, \tag{6}$$

where α is the actual wavenumber. Therefore, the optimization problem is to minimize the L_2 norm of the difference between the numerical wavenumber and the actual wavenumber for a particular wavenumber range $[-\alpha_0\Delta x, \alpha_0\Delta x]$. To be more specific, we seek c_{rj} so that they satisfy Eq. (5) and minimize the integral

$$E_r = \int_{-\alpha_0\Delta x}^{\alpha_0\Delta x} \{\lambda[\text{Re}(\bar{\alpha}^r\Delta x) - \alpha\Delta x]^2 + (1 - \lambda)[\text{Im}(\bar{\alpha}^r\Delta x)]^2\} d(\alpha\Delta x), \tag{7}$$

where E_r is the error to be minimized; parameter λ is chosen to be between 0 and 1 to balance the errors in the real and the imaginary parts. The imaginary part is a measure

of the amplitude error, while the real part indicates the phase error. For a nondissipative central difference scheme, the imaginary part of the numerical wavenumber diminishes, and the minimization problem is simplified. Interested readers should refer to [23] for more information on the central DRP schemes. For upwind optimized schemes, refer to [16, 27, 28] for details.

The design philosophy for ENO schemes [6] is very different from that for the optimized schemes. ENO schemes were developed primarily for high-accuracy capturing of discontinuities or steep gradients. This was achieved through “adaptive stencil,” namely to change the left shift r with the location x_i depending on the smoothness of the local solution to avoid the discontinuity if possible. Note that in selecting the ENO stencil of k points, the field data at $2k - 1$ points is scanned. If one uses all the data scanned in the selection process, one can achieve a maximum $(2k - 1)$ th order of accuracy if the solution on the $2k - 1$ points is smooth. This is exactly the idea used in the WENO schemes. Instead of using only one of the candidate stencils to form the numerical flux, one uses a convex combination of all of them, i.e.,

$$\hat{u}_{i+1/2}^{\text{WENO}} = \sum_{r=0}^{k-1} w_r \tilde{u}_{i+1/2}^r \quad (8)$$

where w_r are the weights, $w_r \geq 0$, and

$$\sum_{r=0}^{k-1} w_r = 1.$$

Apparently the key to the success of WENO schemes would be the choice of the weights w . Based on a Taylor expansion, we can compute a set of weights, denoted by d_r , which achieves the maximum $(2k - 1)$ th order of accuracy. Then for the WENO flux to achieve the maximum order of accuracy, the weights should satisfy the following accuracy requirement if the solution is smooth over all stencils:

$$w_r = d_r + O(\Delta x^{r-1}). \quad (9)$$

In [9], the weights

$$w_r = \frac{\delta_r}{\sum_{r=0}^{k-1} \delta_r}, \quad \delta_r = \frac{d_r}{(\varepsilon + \beta_r)^2}, \quad (10)$$

$$\beta_r = \sum_{l=1}^{k-1} \int_{x_{i-1/2}}^{x_{i+1/2}} \Delta x^{2l-1} \left(\frac{\partial^l p_r(x)}{\partial^l x} \right)^2 dx, \quad r = 0, \dots, k-1$$

were developed, where $p_r(x)$ is the *constructed* polynomial of $(k - 1)$ th order over the interval $[x_{i-1/2}, x_{i+1/2}]$, ε is a small number preventing the denominator to be zero, and according to Fedkiw *et al.* [3], serves as a blending coefficient between the maximum order central scheme and ENO schemes, and β_r is the smoothness indicator. The smoothness indicators for $k = 2, 3$ are given in [9], and the indicators for $k = 4 - 6$ are given in [1]. A sufficient condition [9] for the weights in (10) to satisfy (9) is

$$\beta_r = D(1 + O(\Delta x^{r-1})), \quad (11)$$

where D is some nonzero quantity independent of r .

3. OPTIMIZED WENO SCHEMES

With the descriptions on optimized, ENO, and WENO schemes, it is then straightforward to present the OWENO schemes. The OWENO schemes are developed in the following two major steps.

Step 1. Given the stencil size k , develop optimized schemes achieving p_1 th order of accuracy ($p_1 \leq k$) for all the k candidate stencils

$$\{x_{i-r}, \dots, x_{i+k-r-1}\}, \quad r = 0, 1, \dots, k - 1. \tag{12}$$

By satisfying (5), p_1 linear equations of the following form can be obtained about c_{rj}

$$\sum_{j=0}^{k-1} b_{lj}c_{rj} = z_l, \quad \text{for } l = 1, \dots, p_1, \tag{13}$$

where b_{lj} and z_l are constants. The rest of the $k - p_1$ free parameters are determined by minimizing E_r in (7). E_r is a function of the coefficients c_{rj} ,

$$E_r = E_r(c_{r0}, \dots, c_{r,k-1}). \tag{14}$$

Equations (13) can be used to eliminate p_1 coefficients. Without loss of generality, we assume that the first p_1 coefficients c_{rj} , $j = 0, p_1 - 1$ are eliminated, and they can be expressed as functions of the last $k - p_1$ parameters. Substituting these expressions into (14), we obtain

$$E_r = E_r(c_{r,p_1}, \dots, c_{r,k-1}). \tag{15}$$

To minimize E_r , the following conditions must be satisfied:

$$\frac{\partial E_r}{\partial c_{rj}} = 0, \quad \text{for } j = p_1, \dots, k - 1. \tag{16}$$

Equations (16) would give the desired solution for the remaining coefficients.

Step 2. These optimized schemes for all the k candidate stencils are then convexly combined to obtain the OWENO schemes. More specifically, we first seek constants h_r in the combination

$$\tilde{u}_{i+1/2}^{\text{OWENO}} = \sum_{r=0}^{k-1} h_r \tilde{u}_{i+1/2}^r$$

so that if the solution is smooth over all candidate stencils, we have

$$\frac{1}{\Delta x} (\tilde{u}_{i+1/2}^{\text{OWENO}} - \tilde{u}_{i-1/2}^{\text{OWENO}}) = \left(\frac{\partial u}{\partial x} \right)_i + O(\Delta x^{p_1+p_2}) \tag{17}$$

with $\sum_{r=0}^{k-1} h_r = 1$, $h_r \geq 0$, and $p_2 \leq k - 1$. Equation (17) can be used to determine p_2

TABLE I
 $p_1 = 2, p_2 = 1$ (3rd Order OWENO)

j	$r = 0$	$r = 1$	$r = 2$	$r = 3$	
c_{rj}	0	0.28418590	-0.10076912	0.10019444	-0.27941025
	1	1.0318226	0.60076912	-0.41620299	0.98165507
	2	-0.41620299	0.60076912	1.0318226	-1.6250794
	3	0.10019444	-0.10076912	0.28418590	1.9228346
h_r		0.14150117	0.48616615	0.33383476	0.038497919

weights, leaving $k - 1 - p_2$ weights as free parameters. These free parameters can then again be determined by minimizing an integral in the form of Eq. (7), but with $\bar{\alpha}^r$ replaced by $\bar{\alpha} = \sum_{r=0}^{k-1} h_r \bar{\alpha}^r$. The approach in determining parameters h_r is very similar to the procedure in determining c_{rj} in Step 1. Since h_r is determined assuming the solution is smooth, it is not suitable when the solution has a discontinuity in one or more of the candidate stencils. We again use the smoothness indicators presented in (10) with d_r replaced by h_r .

Performance tests with these smoothness indicators will be presented later. It will be shown that these weights are not suitable for short waves because they cannot distinguish short waves with 6 PPW from discontinuities. A new set of weights will be presented in a later section.

In this paper we constructed a variety of schemes with different stencil sizes, and order of accuracy. In our optimization, we have selected $\lambda = 0.5$ to minimize both the dissipation and the dispersion errors and $\alpha_0 \Delta x = 0.35\pi$. The selection of $\alpha_0 \Delta x = 0.35\pi$ optimizes the schemes for waves with about 6 PPW. The coefficients for some of the OWENO schemes with $k = 4$ are listed in Tables I–IV. Figures 1–3 show the comparison of the relative wavenumber errors among the OWENO schemes of different orders of accuracy and the seventh-order accurate WENO scheme with the same stencil (without the smoothness indicators). Lele [11] defines the resolving efficiency as the fraction of the range of wavenumbers such that the error is below some tolerance τ . If the tolerance is set to be 0.01, then the resolving efficiency of the first-order OWENO scheme is $1.45/\pi = 0.46$ (corresponding to 4.3 PPW), the resolving efficiency of the third-order OWENO scheme is $1.46/\pi = 0.46$ (4.3 PPW), the resolving efficiency of the fifth-order OWENO scheme is $1.22/\pi = 0.39$ (5.2 PPW), and the resolving efficiency of the seventh-order WENO scheme is $1.25/\pi = 0.40$ (5.0 PPW). However, if higher accuracy is required, e.g., $\tau = 0.001$, then the resolving efficiency of the first-order OWENO scheme is $1.15/\pi = 0.37$ (corresponding to 5.5 PPW), the resolving efficiency of the third-order OWENO scheme is $1.16/\pi = 0.37$ (5.5 PPW), the resolving efficiency of the fifth-order OWENO scheme is $0.82/\pi = 0.26$ (7.7 PPW), and the resolving efficiency of the seventh-order WENO scheme is $0.86/\pi = 0.27$ (7.3 PPW). It is interesting to see that the fifth-order OWENO scheme has a lower resolving efficiency than the maximum-order, nonoptimized seventh-order WENO scheme. On the other hand, the first-order and third-order OWENO schemes do have better resolving efficiency than the WENO scheme for $k = 4$. Since the third-order OWENO scheme has a higher formal order of accuracy, and a slightly better resolving efficiency, it is selected in all the numerical computations to be presented later.

TABLE II
 $\mathbf{p}_1 = 1, \mathbf{p}_2 = 0$ (1st Order OWENO)

j	$r = 0$	$r = 1$	$r = 2$	$r = 3$	
c_{rj}	0	0.28950603	-0.10076912	0.094874312	-0.24051909
	1	1.0204113	0.60076912	-0.40479166	0.89823611
	2	-0.40479166	0.60076912	1.0204113	-1.5416604
	3	0.094874312	-0.10076912	0.28950603	1.8839434
h_r		0.15024393	0.48017755	0.32988027	0.039698251

TABLE III
 $\mathbf{p}_1 = 3, \mathbf{p}_2 = 2$ (5th Order OWENO)

j	$r = 0$	$r = 1$	$r = 2$	$r = 3$	
c_{rj}	0	0.25866239	-0.083333333	0.074670939	-0.18445575
	1	1.0573462	0.58333333	-0.39067948	0.88670057
	2	-0.39067948	0.58333333	1.0573462	-1.7200339
	3	0.074670939	-0.083333333	0.25866239	2.0177891
h_r		0.14196688	0.51976365	0.31535440	0.022915068

TABLE IV
 $\mathbf{p}_1 = 4, \mathbf{p}_2 = 3$ (7th Order WENO)

j	$r = 0$	$r = 1$	$r = 2$	$r = 3$	
c_{rj}	0	1/4	-1/12	1/12	-1/4
	1	13/12	7/12	-5/12	13/12
	2	-5/12	7/12	13/12	-23/12
	3	1/12	-1/12	1/4	25/12
h_r		4/35	18/35	12/35	1/35

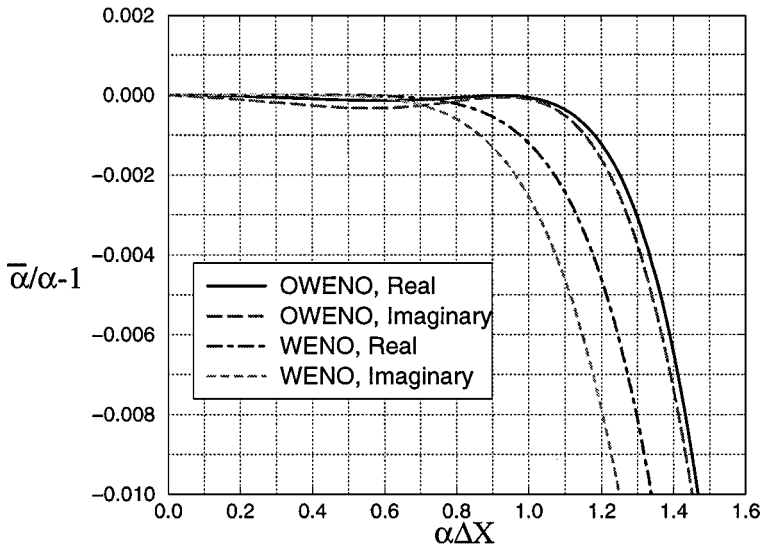


FIG. 1. Comparison of relative wavenumber errors between the seventh-order WENO scheme and the first-order OWENO scheme with $\mathbf{p}_1 = 1$, and $\mathbf{p}_2 = 0$.

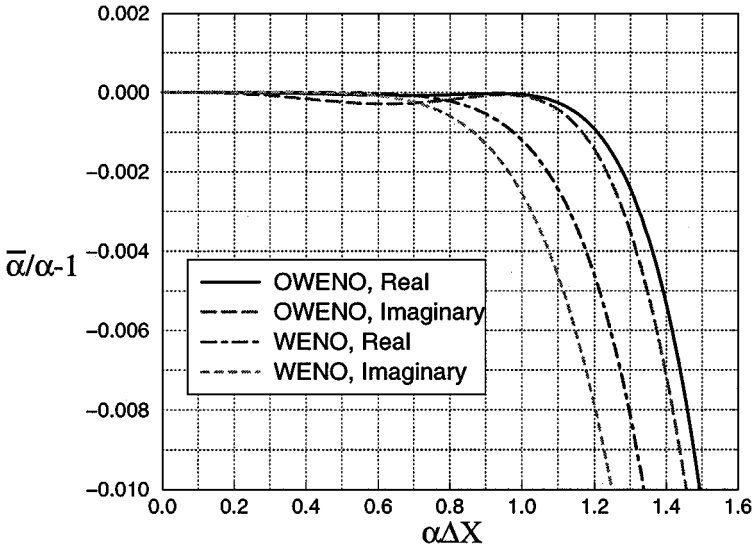


FIG. 2. Comparison of relative wavenumber errors between the seventh-order WENO scheme and the third-order OWENO scheme with $p_1 = 2$, and $p_2 = 1$.

4. EXTENSION TO THE LINEARIZED EULER EQUATIONS

The unsteady Euler equations in conservation form in quasi-1-D can be written as

$$\frac{\partial Q}{\partial t} + \frac{\partial F}{\partial x} = H, \quad (18)$$

where Q is the vector of conserved variables, F is the inviscid flux vector, and H is the

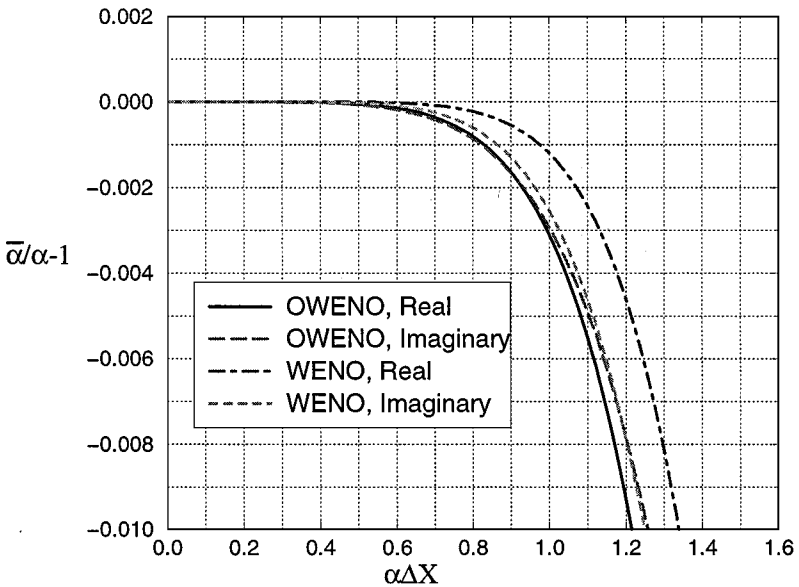


FIG. 3. Comparison of relative wavenumber errors between the seventh-order WENO scheme and the fifth-order OWENO scheme with $p_1 = 3$, and $p_2 = 2$.

vector for the source terms given below:

$$Q = A\{\rho, \rho u, E\}^T, \quad F = A\{\rho u, \rho u^2 + p, u(E + p)\}^T, \quad H = \left\{0, p \frac{\partial A}{\partial x}, 0\right\}^T. \quad (19)$$

Here ρ is density, u is the velocity, p is the pressure, E is the total energy, and A is the area of the cross section. Pressure is related to the total energy by

$$E = \frac{p}{\gamma - 1} + \frac{1}{2}\rho u^2$$

with $\gamma = 1.4$ for air. The linearized Euler equations can be derived by letting

$$p = p_0 + p', \quad \rho = \rho_0 + \rho', \quad u = u_0 + u', \quad (20)$$

where the quantities with subscript 0 are the mean flow values, while those with ' are perturbations. Substituting (20) into (18), and eliminating high-order terms with respect to the perturbations, we obtain the linearized Euler equations. The linearized Euler equations can be written in two forms, one in conservation form, and the other in nonconservation form. The nonconservation linearized Euler equations in transformed coordinate $\xi = \xi(x)$ can be written as

$$\frac{\partial q}{\partial t} + \left(J \frac{\partial q}{\partial \xi} \right) \frac{\partial \xi}{\partial x} = S, \quad (21)$$

where $q = \{\rho', u', p'\}$, J is the Jacobian matrix, and S contains the vector of sources, which are functions of the mean flow variables, their first derivatives, and nozzle area derivatives. The OWENO scheme for equation (21) takes the following form:

$$\frac{\partial q_i}{\partial t} + \frac{1}{\Delta \xi} [J_i^+ (\tilde{q}_{i+1/2}^- - \tilde{q}_{i-1/2}^-) + J_i^- (\tilde{q}_{i+1/2}^+ - \tilde{q}_{i-1/2}^+)] \left(\frac{d\xi}{dx} \right)_i = S_i. \quad (22)$$

Here, each component of $\tilde{q}_{i+1/2}^-$ is computed using the procedure presented in the last section, which assumes that the wave travels in the positive x -direction. Each component of $\tilde{q}_{i+1/2}^+$ is computed in a symmetric fashion assuming the wave travels in the negative x -direction. The Jacobian matrix J can be decomposed into two parts, $J = J^+ + J^-$, with J^+ containing only nonnegative eigenvalues and J^- only nonpositive eigenvalues. The following equation is used to decompose J :

$$J^+ = \frac{1}{2} R_J (\Lambda_J + |\Lambda_J|) R_J^{-1}, \quad J^- = \frac{1}{2} R_J (\Lambda_J - |\Lambda_J|) R_J^{-1},$$

where R_J is composed of the right eigenvectors of J , and Λ_J is a diagonal matrix containing the eigenvalues of J . Note that the nonconservative linearized Euler equations have the first derivatives of the mean flow in the source terms, which become singular if the mean flow has a discontinuity. To handle discontinuous mean flow, one must use the conservation form

$$\frac{\partial U}{\partial t} + \frac{\partial G}{\partial x} = \Theta, \quad (23)$$

where U is the conserved perturbation variables, G is the flux vector, and Θ is the source vector. Let the Jacobian matrix be B , i.e.,

$$B = \frac{\partial G}{\partial U}.$$

Now the source term does not contain the derivatives of mean flow variables. The mean flow is again obtained analytically. Define left and right propagating flux vectors as

$$G^- = 0.5[G - \max |\lambda^l(B)|U] \quad G^+ = 0.5[G + \max |\lambda^l(B)|U] \quad (24)$$

where $\lambda^l, l = 1, 2, 3$ are three eigenvalues of matrix B . We then apply the OWENO scheme to Eq. (23) in the following manner:

$$\frac{\partial U_i}{\partial t} + \frac{1}{\Delta x}(\tilde{G}_{i+1/2} - \tilde{G}_{i-1/2}) = \Theta_i \quad \tilde{G}_{i+1/2} = \tilde{G}_{i+1/2}^- + \tilde{G}_{i+1/2}^+. \quad (25)$$

Each component of G^+ is computed using the procedure presented in the last section assuming that the wave travels in the positive x -direction, and symmetrically the components of G^- can be computed. For the inlet and exit boundary conditions, we follow the approach developed in [23]. One-sided optimized schemes are used to maintain the solution accuracy near boundaries.

5. TIME-INTEGRATION

After proper spatial discretizations, the conservation laws reduce to either a scalar or a system of ordinary differential equations in time, which can be written in the form:

$$\frac{dQ}{dt} = L(Q). \quad (26)$$

In this study a third order TVD Range-Kutta method developed in [20] is employed, which can be written as:

$$\begin{aligned} Q^{(1)} &= Q^n + \Delta t L(Q^n) \\ Q^{(2)} &= \frac{3}{4}Q^n + \frac{1}{4}Q^{(1)} + \frac{1}{4}\Delta t L(Q^{(1)}) \\ Q^{n+1} &= \frac{1}{3}Q^n + \frac{2}{3}Q^{(2)} + \frac{2}{3}\Delta t L(Q^{(2)}) \end{aligned} \quad (27)$$

6. TEST WITH LINEAR WAVE EQUATION AND NEW SMOOTHNESS INDICATORS

To verify the designed advantages of OWENO schemes, we first tested the 7th order WENO and 3rd order OWENO schemes for the linear wave equation (1) with $a = 1$. In the first case a sine wave

$$u_0(x) = \sin\left(\frac{\pi}{3}x\right)$$

was specified in the computational domain and propagated with periodic boundary conditions. We initially turned off the ‘‘smoothness indicators’’ in both WENO and OWENO schemes since the solution was smooth. The computational domain for this case was set to be $[-18, 18]$ with grid size $\Delta x = 1$, i.e., 6 PPW. The time step was set at $\Delta t = 0.1$ to minimize the effects of the time-integration scheme. The simulation was then carried out until $t = 60$. By then, the sine wave traveled for 10 wavelengths. Figure 4a shows

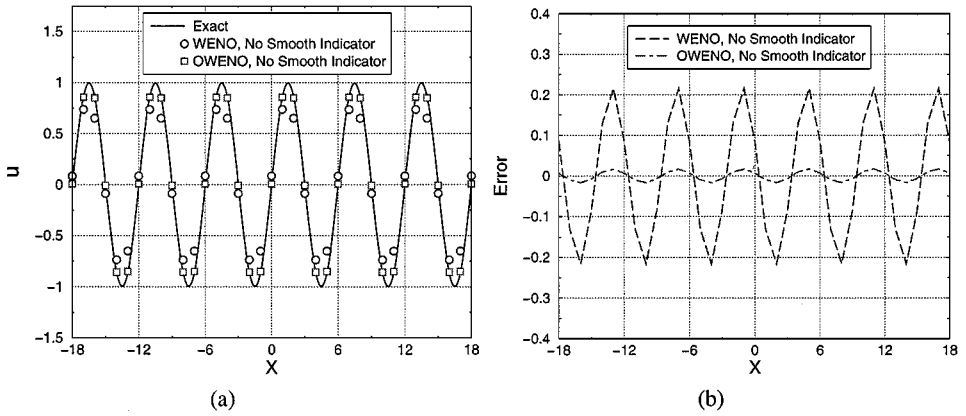


FIG. 4. Comparison of WENO and OWENO schemes for the propagation of a sine wave without the smoothness indicators.

the comparison of the solutions with the WENO and OWENO schemes to the exact solution. The solution errors are compared in Fig. 4b. Note that the solution error obtained with the OWENO scheme is significantly lower (by more than an order of magnitude) than that with WENO. Next, we turned on the smoothness indicators with everything else remaining exactly the same. The solutions with both WENO and OWENO schemes are compared to the exact solution in Fig. 5a, and the solution errors are shown in Fig. 5b. Again, the solution error with the OWENO scheme is much lower than that with WENO. However, the errors with both schemes are significantly higher than those without smoothness indicators. This case clearly indicates that the smoothness indicators “thought” that the sine wave at six grid-spacings per-wave was actually discontinuous, and therefore were turned on. Therefore, significant numerical dampings were added in the solution, as is evident in Fig. 5. If we are to develop proper OWENO schemes for short waves, it is critical that the smoothness indicators should not be turned on for short waves. We tested a variety of new smoothness indicators, and found the following one worked the best for

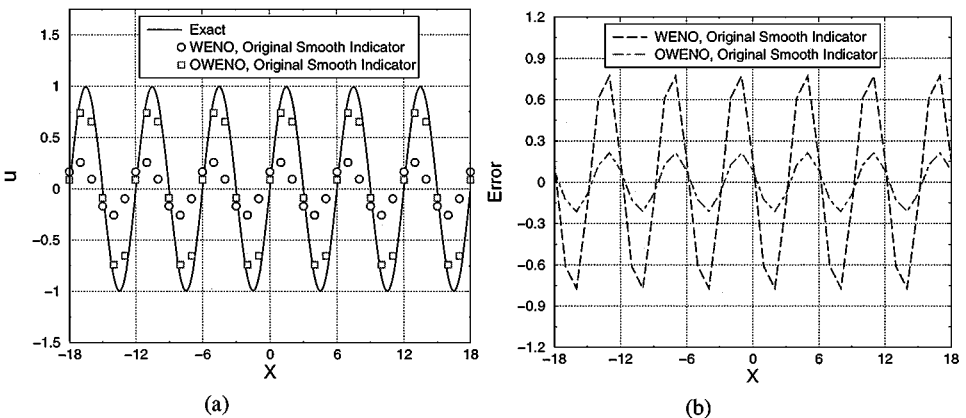


FIG. 5. Comparison of WENO and OWENO schemes for the propagation of a sine wave with the original smoothness indicators in [9].

short waves:

$$\beta_r = \sum_{\substack{l=2 \\ k > 2}}^{k-1} \left[\int_{x_{i-1/2}}^{x_{i+1/2}} \Delta x^{l-1} \frac{\partial^l p_r(x)}{\partial^l x} dx \right]^2, \quad r = 0, \dots, k-1. \quad (28)$$

For $k = 4$, the new smoothness indicators take the following form:

$$\beta_0 = (2u_i - 5u_{i+1} + 4u_{i+2} - u_{i+3})^2 + (-u_i + 3u_{i+1} - 3u_{i+2} + u_{i+3})^2 \quad (29)$$

$$\beta_1 = (u_{i-1} - 2u_i + u_{i+1})^2 + (-u_{i-1} + 3u_i - 3u_{i+1} + u_{i+2})^2 \quad (30)$$

$$\beta_2 = (u_{i-1} - 2u_i + u_{i+1})^2 + (-u_{i-2} + 3u_{i-1} - 3u_i + u_{i+1})^2 \quad (31)$$

$$\beta_3 = (-u_{i-3} + 4u_{i-2} - 5u_{i-1} + 2u_i)^2 + (-u_{i-3} + 3u_{i-2} - 3u_{i-1} + u_i)^2. \quad (32)$$

In smooth regions, Taylor expansion of (29–32) gives

$$\beta_r = (u_i'' \Delta x^2)^2 + (u_i''' \Delta x^3)^2 + O(\Delta x^6), \quad r = 0, \dots, 3. \quad (33)$$

Obviously, if $u_i'' \neq 0$, then

$$\beta_r = (u_i'' \Delta x^2)^2 (1 + O(\Delta x^2)), \quad r = 0, \dots, 3, \quad (34)$$

which is similar to the accuracy requirement given in (11). Equation (34) in fact means that two extra orders of accuracy can be possibly obtained using the new smoothness indicators by convexly combining the optimized schemes. Note that the third-order OWENO scheme was obtained using $p_1 = 2$, and $p_2 = 1$. Therefore, the new set of smoothness indicators should be compatible with the third-order OWENO scheme. To numerically verify this claim, an accuracy study was performed using the third-order OWENO scheme with the new smoothness indicators. The computational domain was set to be $[-1, 1]$, with $u_0(x) = \sin(\pi x)$ and periodic boundary conditions. The simulation was carried out until $t = 1$ with CFL = 0.25. The numerical L_1 and L_∞ errors are presented in Table V. Note that in both norms, third-order accuracy is achieved.

One may argue that if one of the derivatives

$$\frac{\partial^l p_r(x)}{\partial^l x}$$

in (28) is an odd function of $x - x_i$, then the integral of the derivative is zero, thus failing to recognize a possible steep gradient. The counter argument is that for any $k > 3$, the

TABLE V
Accuracy Study with 3rd Order OWENO Scheme

N	L_1 error	L_1 order	L_∞ error	L_∞ order
10	8.59e-3	—	1.41e-2	—
20	8.92e-4	3.27	1.85e-3	2.93
40	4.69e-5	4.25	1.23e-4	3.91
80	5.02e-6	3.22	1.59e-5	2.95
160	5.55e-7	3.18	8.49e-7	4.23
320	6.96e-8	3.00	1.09e-7	2.96

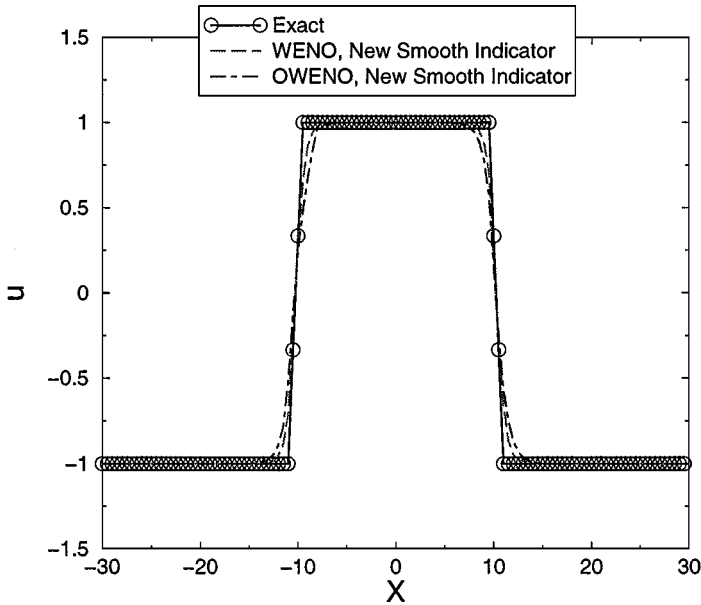


FIG. 6. Simulation of a square wave with a linear shock profile using both WENO and OWENO schemes with the new smoothness indicators.

smoothness indicators consist of the integrals of at least two derivatives. Since $p_r(x)$ is a $(k - 1)$ th order polynomial, if one derivative is an odd function, the other derivative should be an even function. Therefore its integral should not be zero. As a result, the smoothness indicators should still be capable of recognizing a possible steep gradient. A close examination of (29–32) reveals that the smoothness indicators are zero if and only if the solution at the stencil is linear. For example, we have $\beta_0 = 0$ only when $u_i - 2u_{i+1} + u_{i+2} = 0$ and $u_{i+1} - 2u_{i+2} + u_{i+3} = 0$, i.e., the solution is linear in the stencil, in which case the solution in the stencil should not be recognized as a steep gradient. In the case of $k = 3$, $p_r(x)$ is a quadratic function. Its second-derivative is a nonzero constant in most cases which can never be an odd function, unless $p_r(x)$ degenerates into a linear function. In this case, we have again linear data in the stencil, which should not be recognized as a steep gradient. We designed a square wave case with a linear shock profile to test the above argument, i.e., the shock is linearly spread over four grid points as shown in Fig. 6. It is obvious that the smoothness indicator for the stencil containing the linear shock profile is zero. Both the seventh-order WENO and the third-order OWENO schemes were tested for this case with the new smoothness indicators. A total of 121 grid points were generated to cover the domain of $[-30, 30]$. The shock wave was then propagated across the computational domain twice with $\Delta t = 0.1$. The computational solutions with both schemes are compared with the exact solution in Fig. 6. Note that both schemes produced nonoscillatory shock profiles with the new smoothness indicators.

With the new smoothness indicators, the solutions with the WENO and OWENO schemes and their errors for the sine wave are shown in Fig. 7. It is obvious that the solution errors with the new smoothness indicators are reduced significantly compared to those with the original smoothness indicators. The solution errors with and without the smoothness indicators are presented in Fig. 8. Note that the new smoothness indicators do not significantly affect the short waves for both WENO and OWENO schemes. Next, the OWENO scheme was tested

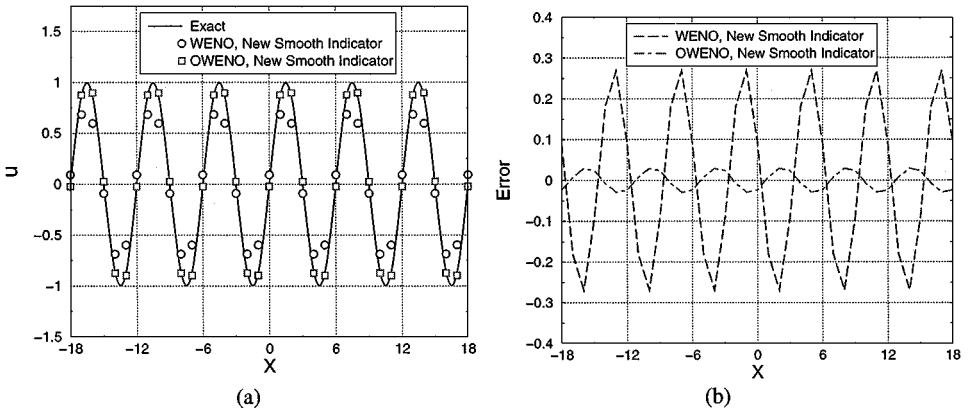


FIG. 7. Comparison of WENO and OWENO schemes for the propagation of a sine wave with the new smoothness indicators.

for an artificial “broadband” wave, which is composed of the following three sine waves as given by

$$u_0(x) = \sin\left(\frac{\pi x}{3}\right) + \sin\left(\frac{\pi x}{6}\right) + \sin\left(\frac{\pi x}{12}\right).$$

The wavelengths of the three waves are 6, 12, and 24, respectively, and they are therefore called short, medium, and long waves. The initial wave form is displayed in Fig. 9. The computational domain was chosen to be $[-12, 12]$ with grid size $\Delta x = 1$ and $\Delta t = 0.1$. The wave then traveled for five short wavelengths until $t = 30$. The solutions with WENO and OWENO schemes are compared with the exact solution in Fig. 10a. The solution errors are shown in Fig. 10b. Again OWENO performed better than WENO as expected for this

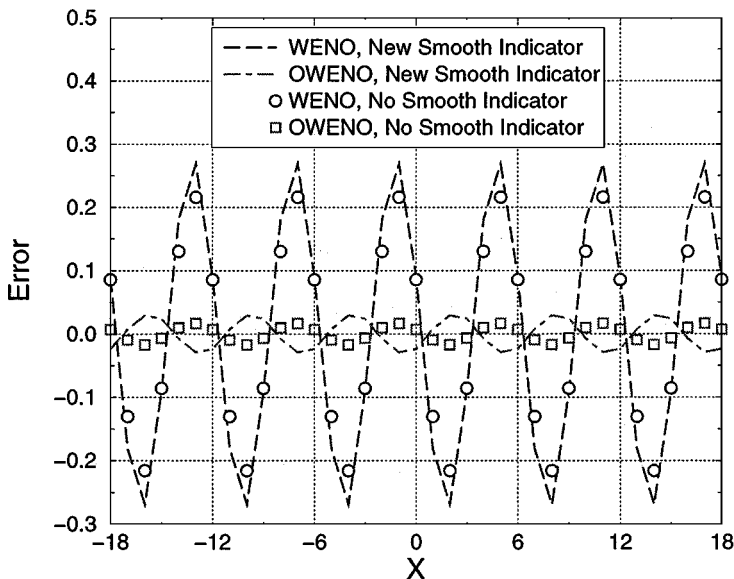


FIG. 8. Comparison of WENO and OWENO schemes for the propagation of a sine wave with the new smoothness indicators and without smoothness indicators.

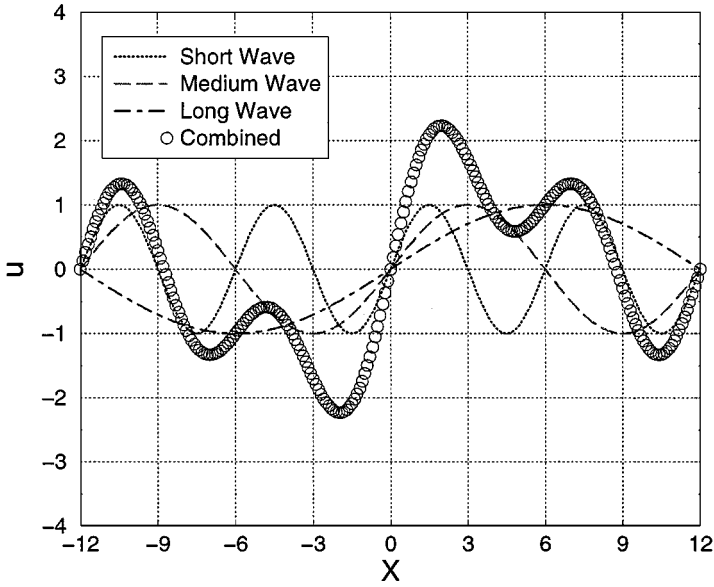


FIG. 9. The formation of a “broadband” wave.

artificial “broadband” wave. After that, we wanted to see how OWENO schemes perform for discontinuities. In this test, a square wave was propagated in the computational domain with periodic boundary conditions. The computational domain was chosen to be $[-30, 30]$ with $\Delta x = 0.5$. The initial wave was specified as

$$u_0 = \begin{cases} 1 & -10 \leq x \leq 10 \\ 0 & \text{otherwise.} \end{cases}$$

The time step Δt was set to 0.1, which is small enough so that the error due to time integration is negligible. The simulation was carried out until $t = 120$. Therefore, the wave was allowed to travel across the computational domain twice. Figure 11 shows the numerical results with the WENO and OWENO schemes using the new smoothness indicators and the exact solution. Note that both WENO and OWENO schemes gave monotonic solutions for the square wave (at least to the naked eyes), although the OWENO scheme

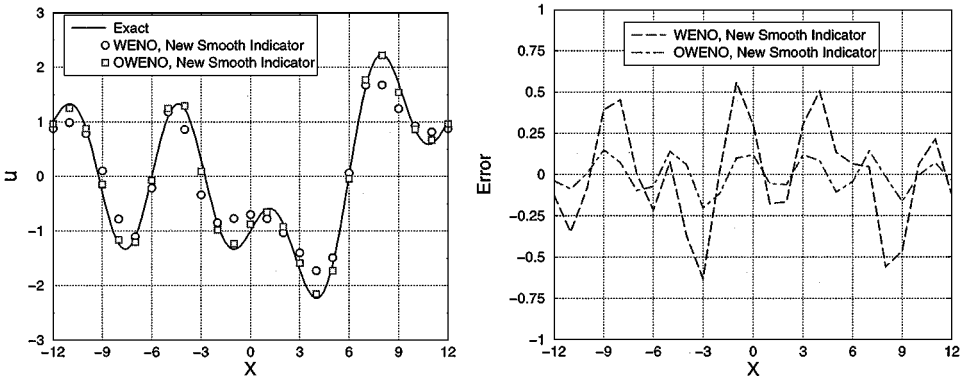


FIG. 10. Comparison of WENO and OWENO schemes for the propagation of a “broadband” wave with the new smoothness indicators.

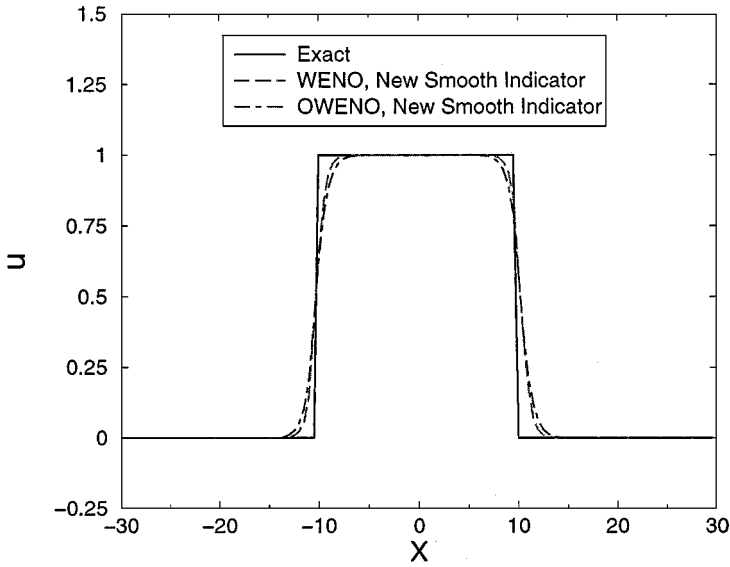


FIG. 11. Comparison of WENO and OWENO schemes for the propagation of a square wave with the new smoothness indicators.

smear the solution slightly more than the WENO scheme. This case also demonstrates that the new smoothness indicators work well for discontinuities. Just to show the comparison between the new and original smoothness indicators for discontinuities, we used both smoothness indicators with the WENO scheme to perform the same simulation. Figure 12 displays the solutions with the original and new smoothness indicators. The solutions are indistinguishable from each other. Finally, to demonstrate the potential of OWENO schemes for shock/acoustic wave interaction problems, the linear combination of a square wave and a sine wave was simulated. The period of the combined wave was 24. The initial wave form

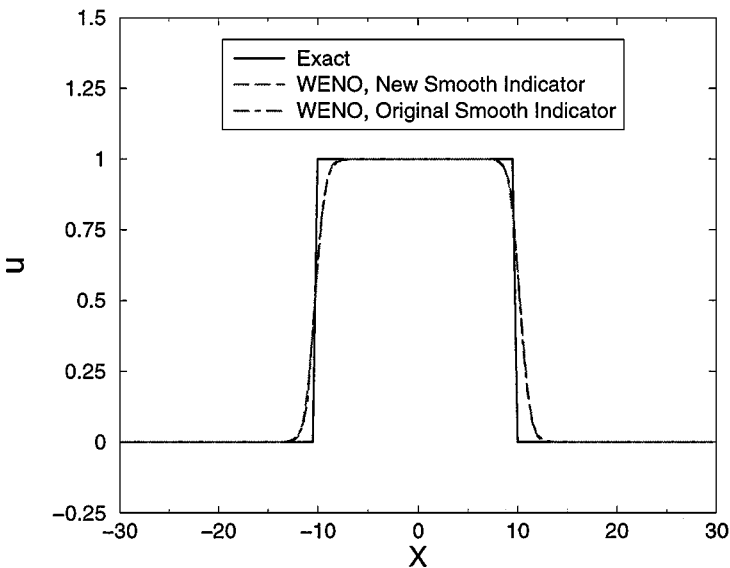


FIG. 12. Comparison of WENO schemes for the propagation of a square wave with the original and new smoothness indicators.

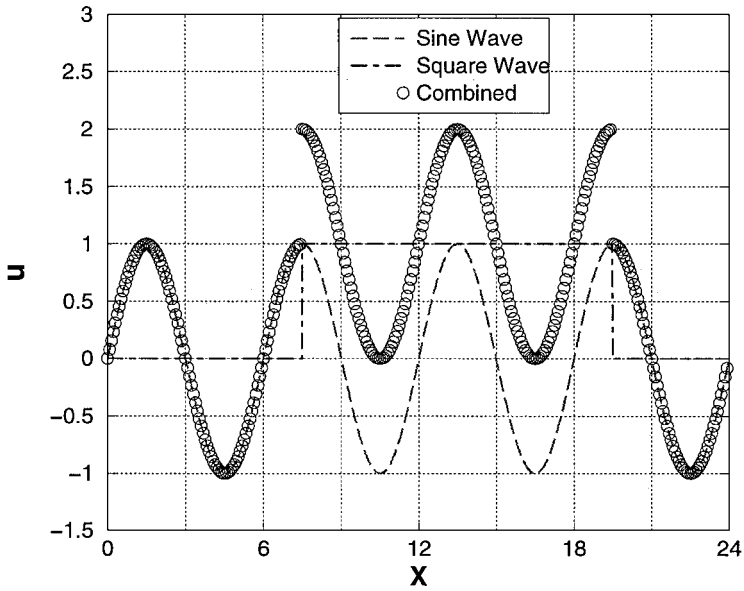


FIG. 13. The formation of a discontinuous sine wave.

was set to be

$$u_0 = \begin{cases} 1 + \sin\left(\frac{\pi x}{3}\right), & 7.5 \leq x < 19.5 \\ \sin\left(\frac{\pi x}{3}\right) & \text{otherwise,} \end{cases}$$

which is displayed in Fig. 13. The computational domain for the case was $[0, 24]$ with $\Delta x = 1$ and $\Delta t = 0.1$. The simulation was carried out until $t = 48$ so that the wave traveled across the computational domain twice. The computed solutions with WENO and OWENO schemes are shown in Fig. 14. Although both schemes smeared the discontinuity heavily

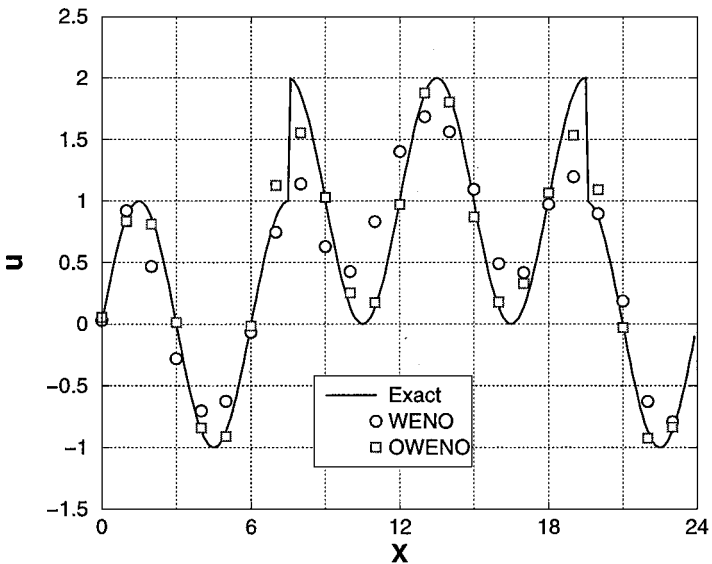


FIG. 14. Comparison of WENO and OWENO schemes for the propagation of a discontinuous sine wave with the new smoothness indicators.

at this grid resolution, it is noted that the smearing of the discontinuity does not affect the resolution for the sine wave that much with the OWENO scheme. For the WENO scheme, however, the resolution for the sine wave is much lower. In practical CAA simulations involving discontinuities, it may not always be possible to resolve the discontinuities with high resolutions. With OWENO schemes, it seems hopeful that the acoustic waves may still be resolved with high resolutions.

7. APPLICATION TO CAA BENCHMARK PROBLEMS

After the advantages of OWENO schemes were verified on the linear wave equation, they were then extended to solve the linearized Euler equations, in both the conservation and nonconservation forms. Two benchmark problems from the Third Computational Aeroacoustics (CAA) Workshop on Benchmark Problems [24] were then solved with the OWENO schemes.

Problem 1. Propagation of Sound Waves through a Transonic Nozzle

This benchmark problem is designed to model acoustic wave propagation through a nozzle where the local Mach number near the throat may be close to 1. The area variation of the nozzle is given by

$$A(x) = \begin{cases} 0.536572 - 0.198086e^{-\ln^2(\frac{x}{0.6})^2}, & x > 0 \\ 1.0 - 0.661514e^{-\ln^2(\frac{x}{0.6})^2}, & x < 0. \end{cases} \quad (35)$$

The governing equations are the linearized quasi-1-D Euler equations. The Mach number in the uniform region downstream of the throat is 0.4. Small amplitude acoustic waves, with angular frequency $\varpi = 0.6\pi$, are generated way downstream and propagate upstream through the narrow passage of the nozzle throat. The upstream-propagating wave in the uniform region downstream of the nozzle throat is represented by

$$\begin{bmatrix} \rho' \\ u' \\ p' \end{bmatrix} = \mu \begin{bmatrix} 1 \\ -1 \\ 1 \end{bmatrix} \cos \left[\varpi \left(\frac{x}{1-M} + t \right) \right], \quad (36)$$

where $\mu = 10^{-5}$. The computational domain is $[-10, 10]$. Since the mean flow is smooth, the nonconservation form linearized Euler equations were used in the simulation. A nonuniform grid with 301 points was employed with a hyperbolic sine transformation. The grid was clustered near the throat, and the ratio between the largest grid spacing to the smallest was about 30. The mean flow was computed analytically. No smoothness indicators were used in the weights because of the smooth mean flow. The time step was set to be 0.005. The simulation started with zero perturbations everywhere until it reached a periodic steady state. Figure 15 displays the exact maximum pressure envelope and the computed pressure distributions at four different times in a period. It is obvious that the pressure distributions are nicely bounded by and touch the exact envelope. The computed pressure envelope is then compared with the exact pressure envelope in Fig. 16. Enlarged views of the same figure near the throat and exist are shown in Fig. 17. Note that the agreement between the computational and exact solutions is excellent.

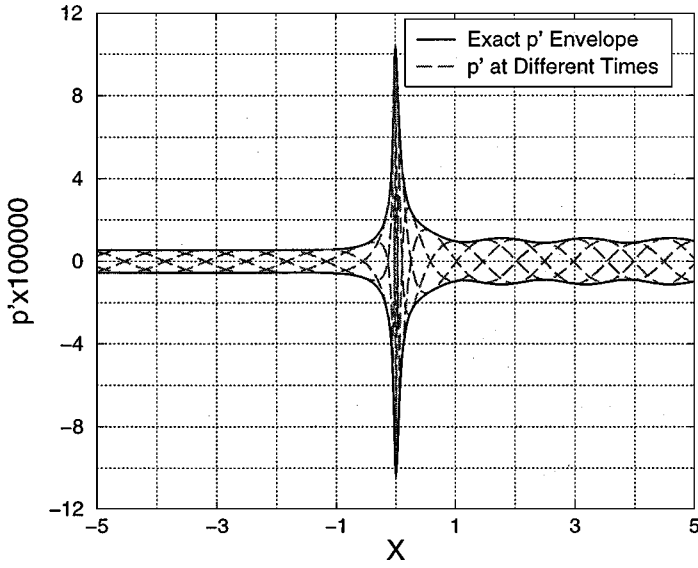


FIG. 15. Comparison between the exact pressure envelope and computed pressure distributions at four different times.

Problem 2. Shock-Sound Interaction

This problem is designed to simulate shock-sound interactions. The geometry is exactly the same as in Problem 1, but now there is a supersonic shock downstream of the throat. The inlet Mach number is $M = 0.2006533$, and the exist pressure is set at 0.6071752 to generate a normal shock downstream of the throat. At the inflow boundary, the

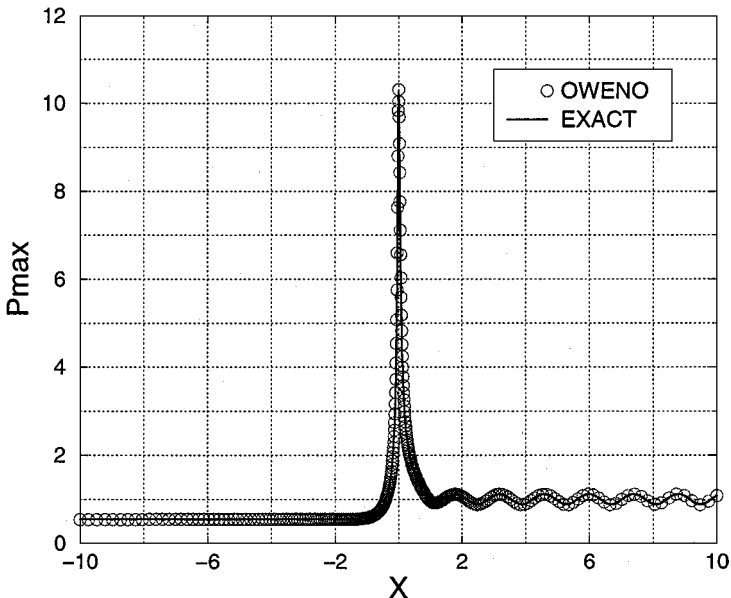


FIG. 16. Comparison between the exact pressure envelope and the computed pressure envelope.

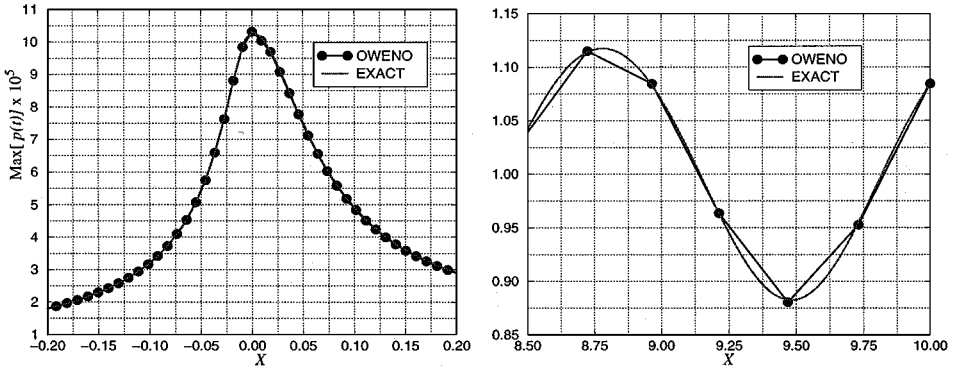


FIG. 17. Comparison of the computed pressure envelope and the exact pressure envelope near the throat and the exit.

conditions are

$$\begin{bmatrix} \rho \\ u \\ p \end{bmatrix} = \begin{bmatrix} 1 \\ M \\ \frac{1}{\gamma} \end{bmatrix} + \mu \begin{bmatrix} 1 \\ 1 \\ 1 \end{bmatrix} \sin \left[\varpi \left(\frac{x}{1+M} - t \right) \right], \quad (37)$$

where $\mu = 10^{-5}$, $\bar{\omega} = 0.6\pi$. Since there was a shock wave in the mean flow, we employed the conservation-form linearized Euler equations. The mean flow was again obtained analytically, and is shown in Fig. 18. A uniform grid with 201 points in the computational domain $[-10, 10]$ was used. A time step of 0.01 was employed in the simulation. We again started the simulation from zero perturbation fields everywhere until the computation reached a periodic steady state. Figure 19 shows the comparison of the computed pressure field using the third-order OWENO scheme with the new smoothness indicators defined in (29–32) and the exact pressure solution at the beginning of a period. The density perturbation was

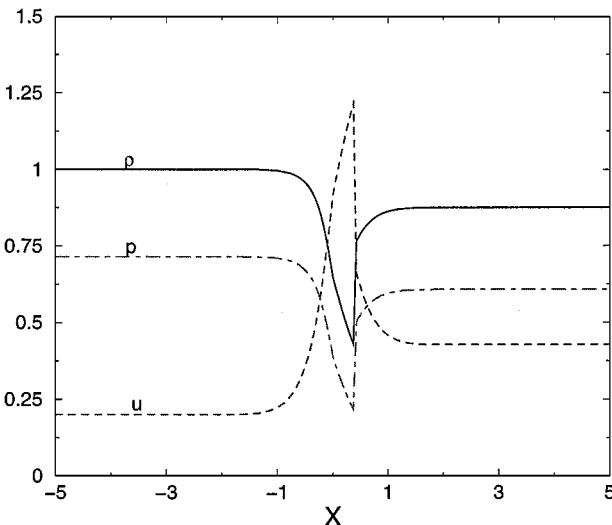


FIG. 18. Mean flow distributions for the case of shock-sound interaction.

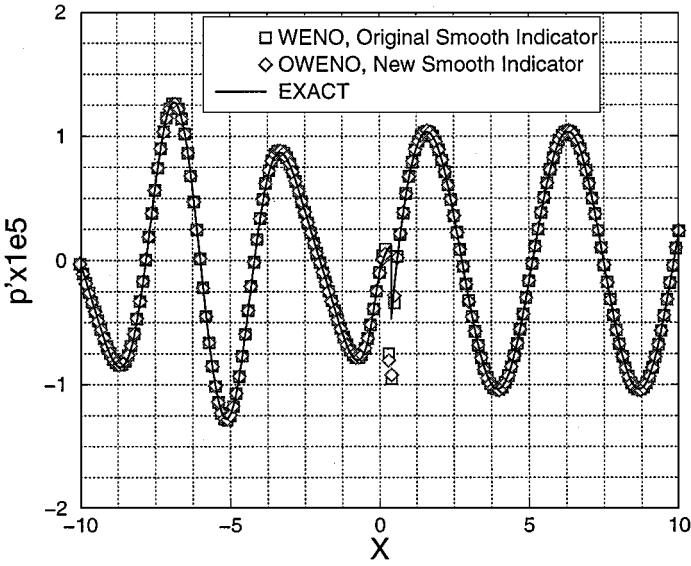


FIG. 19. Comparison of computed pressure distributions with WENO and OWENO schemes and exact solution at the beginning of a period using the conservation-form linearized Euler equations.

used in the smoothness indicators. Note that the agreement between the computational and exact pressure fields is excellent before and after the shock wave. There is, however, a slight overshoot near the shock wave in the computed pressure field. Just for comparison, the same simulation was also performed with the seventh-order WENO scheme and the original smoothness indicators. The computed solutions essentially coincided with each other as shown in Fig. 19. We also used pressure and velocity perturbations in the smoothness indicators, and changed the value of ε in (10) based on the definition given by Fedkiw *et al.* [3]. The solutions shown in Fig. 19 are the best we could obtain. One possible factor for the overshoot is that the extension of the scalar scheme to the linearized Euler equations is done using a split flux approach. According to the recommendations given by Shu [21], an extension based on the characteristic variables may give better predictions near the shock. Future work is necessary to investigate the cause of the oscillation around the shock wave. We also used the nonconservative linearized Euler equations to simulate this case assuming that the shock wave is smeared over one mesh spacing so that finite first derivatives of the mean flow can be calculated near the shock wave. The pressure field after the shock wave was not correctly captured by the nonconservative formulation. This simulation demonstrates the importance of conservation in the computational simulations with discontinuities.

8. CONCLUSIONS

Optimized WENO schemes have been developed in this study to unite the advantages of both the optimized and WENO schemes in the simulation of shock/broadband acoustic waves. By design, OWENO schemes are capable of resolving waves at 6 PPW, while giving essentially nonoscillatory solutions for discontinuities. It was found that the original smoothness indicators developed by Jiang and Shu [9] added significant numerical dampings into the schemes for waves at 6 PPW. New smoothness indicators are developed, and

shown to be compatible with the accuracy requirement. These new smoothness indicators performed much better for waves at 6 PPW than the original ones. They were also tested with discontinuities, and were found to perform as well as the original indicators. Numerical tests with the scalar model wave equation verified the designed advantages of OWENO schemes. The OWENO schemes are then extended to the linearized Euler equations, in both the conservation and nonconservation forms. Two problems in the Third Computational Aeroacoustics (CAA) Workshop on Benchmark Problems were solved with the third-order OWENO scheme. The scheme was found to perform satisfactorily for both problems. It is shown, however, the conservation form linearized Euler equations must be used if the mean flow is discontinuous to capture the proper behavior of the acoustic waves across the shock wave. The implementation of the OWENO schemes for the nonlinear Euler equations is now under way, and will be reported in a future publication.

ACKNOWLEDGMENTS

The authors thank Dr. C.-W. Shu for bringing [13, 26] to their attention. We also acknowledge helpful discussions on smoothness indicators with Dr. C.-W. Shu and Dr. D. S. Balsara.

REFERENCES

1. D. S. Balsara and C.-W. Shu, Monotonicity preserving weighted essentially non-oscillatory schemes with increasingly high-order accuracy, *J. Comput. Phys.* **160**, 405 (2000).
2. J. Casper and H. L. Atkins, A finite volume high-order ENO scheme for two-dimensional hyperbolic systems, *J. Comput. Phys.* **106**, 62 (1993).
3. R. P. Fedkiw, B. Merriman, and S. Osher, Simplified discretization of systems of hyperbolic conservation laws containing advection equations, *J. Comput. Phys.* **157**, 302 (2000).
4. D. Gaitonde and J. S. Shang, Optimized compact-difference-based finite volume schemes for linear wave phenomena, *J. Comput. Phys.* **138**, 617 (1997).
5. A. Harten, High resolution schemes for hyperbolic conservation laws, *J. Comput. Phys.* **49**, 357 (1983).
6. A. Harten, B. Engquist, S. Osher, and S. Chakravarthy, Uniformly high order essentially non-oscillatory schemes III, *J. Comput. Phys.* **71**, 231 (1987).
7. R. Hixon, Evaluation of a high-accuracy MacCormack-type scheme using benchmark problems, NASA Contractor Report 202324, ICOMP-97-03 (1997).
8. A. Jameson, W. Schmidt, and E. Turkel, Numerical solutions of the Euler equations by finite volume methods using Runge-Kutta time-stepping, Technical Paper 81-1259 (AIAA Press, Washington, DC, 1981).
9. G. Jiang and C.-W. Shu, Efficient implementation of weighted ENO schemes, *J. Comput. Phys.* **126**, 202 (1996).
10. C. Kim, P. L. Roe, and J. P. Thomas, Accurate schemes for advection and aeroacoustics, Technical Paper 97-2091 (AIAA Press, Washington, DC, 1997).
11. S. K. Lele, Compact finite difference schemes with spectral-like resolution, *J. Comput. Phys.* **103**, 16 (1992).
12. S. Y. Lin and Y. S. Chin, Comparison of higher resolution Euler schemes for aeroacoustics computations, *AIAA J.* **33**, 237 (1995).
13. S. Y. Lin and J. J. Hu, Parameter study of weighted essentially non-oscillatory schemes for computational aeroacoustics, *AIAA J.* **39**, 371 (2001).
14. X. D. Liu, S. Osher, and T. Chan, Weighted essentially non-oscillatory schemes, *J. Comput. Phys.* **115**, 200 (1994).
15. Y. Liu, Fourier analysis of numerical algorithms for the Maxwell equations, *J. Comput. Phys.* **124**, 396 (1996).
16. D. P. Lockard, K. S. Brentner, and H. L. Atkins, High-accuracy algorithms for computational aeroacoustics, *AIAA J.* **33**, 246 (1995).

17. S. Osher and S. Chakravarthy, Upwind schemes and boundary conditions with applications to Euler equation in general geometries, *J. Comput. Phys.* **50**, 447 (1983).
18. P. L. Roe, Approximate Riemann solvers, parameter vectors, and difference schemes, *J. Comput. Phys.* **43**, 357 (1981).
19. L. N. Sankar, N. N. Reddy, and N. Hariharan, A third order upwind scheme for aeroacoustic application, Technical Paper 93-0149 (AIAA Press, Washington, DC, 1993).
20. C.-W. Shu, Total-variation-diminishing time discretizations, *SIAM J. Sci. Stat. Comput.* **9**, 1073 (1988).
21. C.-W. Shu, Essentially non-oscillatory and weighted essentially non-oscillatory schemes for hyperbolic conservation laws, in *Advanced Numerical Approximation of Nonlinear Hyperbolic Equations*, B. Cockburn, C. Johnson, C.-W. Shu, and E. Tadmor (Edited by A. Quarteroni), Lecture Notes in Mathematics (Springer-Verlag, Berlin/New York, 1998), Vol. 1697, pp. 325–432.
22. C. K. W. Tam, Computational aeroacoustics: issues and methods, *AIAA J.* **33**, 1788 (1995).
23. C. K. W. Tam and J. C. Webb, Dispersion-relation-preserving finite difference schemes for computational acoustics, *J. Comput. Phys.* **107**, 262 (1993).
24. C. K. W. Tam, L. N. Sankar, and D. L. Huff, Third Computational Aeroacoustics (CAA) Workshop on Benchmark Problems, Cleveland, Ohio, November 1999.
25. B. van Leer, Towards the ultimate conservative difference scheme V. A second order sequel to Godunov's method, *J. Comput. Phys.* **32**, 101 (1979).
26. V. G. Weirs and G. V. Candler, Optimization of weighted ENO schemes for DNS of compressible turbulence, Technical Paper 97-1940 (AIAA Press, Washington, DC, 1997).
27. M. Zhuang and R. F. Chen, Optimized upwind dispersion-relation-preserving finite difference schemes for computational aeroacoustics, *AIAA J.* **36**, 2146 (1998).
28. M. Zhuang and R. F. Chen, Applications of the optimized upwind dispersion relation preserving schemes for multi-dimensional acoustic problems. Technical Paper 98-2367 (AIAA Press, Washington, DC, 1998).
29. D. W. Zingg, A review of high-order and optimized finite-difference methods for simulating linear wave phenomena, Technical Paper 97-2088 (AIAA Press, Washington, DC, 1997).